Axial Momentum Lost to a Lateral Wall of a Helicon Plasma Source

Kazunori Takahashi,* Aiki Chiba, Atsushi Komuro, and Akira Ando
Department of Electrical Engineering, Tohoku University, Sendai 980-8579, Japan
(Received 15 January 2015; published 12 May 2015)

Momentum exerted to a lateral wall of a helicon plasma source is individually measured for argon, krypton, and xenon gases. A significant loss of the axial plasma momentum to the lateral wall, which has been assumed to be negligible, is experimentally identified when an axially asymmetric density profile is formed in the source. This indicates that the radially lost ions deliver not only the radial momentum but also the axial momentum to the lateral wall. The formation of the axial asymmetry causing the momentum loss is interpreted with competition between the magnetic field and neutral depletion effects.

DOI: 10.1103/PhysRevLett.114.195001 PACS numbers: 52.30.-q, 52.70.-m, 52.75.Di

The momentum of charged particles in plasmas is one of the crucial parameters associated with acceleration, transport, and confinement of naturally occurring [1,2] and artificial [3,4] plasmas. It is also an essential parameter to model the plasma characteristics in the laboratory [5] and to assess the performance of plasma thrusters [6]. The imparted thrust is equal in magnitude and opposite in direction to the exhausted axial plasma momentum, where the force exerted on the thruster structures (including the mechanical structures and magnetic fields) corresponds to the thrust in laboratory experiments. Hence the measurement of the thrust is equivalent to a direct identification of the plasma momentum. In artificial plasma devices such as the thrusters, low-temperature plasma devices, and fusion reactors, the momentum interaction with the physical boundaries is a critical problem—as is that with electromagnetic fields—to model the plasma behavior according to a momentum balance.

A helicon plasma thruster (HPT) is a recently investigated electrodeless propulsion device [7] consisting of a helicon source [8,9] and a magnetic nozzle. The process of electrostatic ion acceleration and electromagnetic plasma acceleration in magnetically expanding helicon plasmas have been experimentally observed by measuring ion energy distribution [10–12] and by measuring a magnetic force acting to the magnetic nozzle [13], respectively. A one-dimensional model has shown that the electric field leading to the electrostatic ion acceleration does not impart momentum to the plasma, while the axial plasma momentum increases along the magnetic nozzle via the electromagnetic acceleration and hence the thrust also increases [6]. The presence of the magnetic thrust has also been shown in two-dimensional models [13,14].

The production and expansion regions are sometimes connected in theoretical models [15,16] to derive the thruster performance, where the energy balance, the momentum balance, or both in the source cavity give the plasma parameters in the source and the magnetic force is derived for the given plasma injection into the nozzle. Plasma cross-field diffusion affects both the plasma property in the source and the magnetic thrust in the nozzle. The former has been studied theoretically [15–17] and a critical magnetic field for transporting the plasma to the source exit is experimentally observed [18], while the latter has been investigated experimentally by changing the magnetic field strength [19]. The plasma inside the source cavity has also been shown to be affected by a neutral depletion theoretically [5,15] and in laboratory experiments [20,21]. The recent models have suggested that the present inefficient HPT performance results from the energy loss to the lateral wall [15,16].

In the thruster models, the total thrust is given by the sum of three terms: pressure force to the source back plate (T_s), force to the lateral wall (T_w), and the Lorentz force to the magnetic nozzle (T_B), where the detailed expression in a simple electron-diamagnetic model can be found in Ref. [19]. The term T_w is again shown here as

$$T_w = -2\pi \int r_s m n(r_s, z) u_r(r_s, z) u_z(r_s, z) dz, \quad (1)$$

where r_s, m, n, u_r, and u_z are the radius of the lateral wall, the ion mass, the density, and the radial and axial ion velocities, respectively. The integration in Eq. (1) should be performed from the upstream back plate position to the open source exit. This term implies the axial momentum (mu_z for each ion) delivered by radially lost ions with the flux $n_w u_r$ and has been assumed to be negligible, since the ions near the lateral wall are considered to be axially slow and do not deliver significant axial momentum [16,22]. Even in the two-dimensional model giving plasma characteristics in the source, the momentum balances in the radial and axial directions have been decoupled by neglecting the radial variation of the axial momentum [15], which at the lateral wall corresponds to the T_w term in the thruster model.

Here a significant loss of the axial momentum to the lateral wall (the negative value of T_w) is experimentally

detected, where the HPT is operated in argon, krypton, and xenon. It is observed that the momentum loss increases when using the heavier gas species. Since the presence of the non-negligible T_w term affects the momentum balance in steady-state plasmas, it is a crucial problem to model laboratory bounded plasmas as well as the HPT performance.

Experiments are performed with the setup in Fig. 1(a), being very similar to the previous experiment [19], where the difference from the previous setup is only that the source tube is changed from a 6.4-cm-inner-diameter Pyrex tube into a 6-cm-inner-diameter ceramic tube for thermal issue. The HPT consists of the ceramic tube source cavity (the lateral wall), the source back plate located at $z = -20$ cm and mechanically isolated from the lateral wall, a solenoid centered at $z = -3.5$ cm and providing the magnetic nozzle, and a double-turn rf loop antenna wound around and mechanically isolated from the ceramic tube. The HPT and a pendulum force balance are immersed in a 60-cm-diameter and 140-cm-long vacuum chamber, which is pumped down to a base pressure of 10^{-6} Torr. Here the axial location of the open source exit is defined as $z = 0$. The back plate has a small center hole and either argon, krypton, or xenon is introduced into the cavity through the center hole. The mass flow rates of the gases are maintained at 0.75 mg/s for all of the gas species. Then the pressures measured at the chamber side wall are 0.7 mTorr for argon, 0.5 mTorr for krypton, and 0.3 mTorr for xenon. The axial profile of the magnetic field strength B_z for a solenoid current of $I_B = 1$ A is plotted in Fig. 1(b). The profile has the maximum magnetic field strength of ~50 G/A at $z = -3.5$ cm and decreases to about ~5 G/A at both $z \sim 10$ cm and $z \sim -16$ cm. The rf antenna ($z = -11.5$ cm) is powered by a 13.56 MHz and 1 kW rf generator through an impedance matching circuit. The plasma density and the electron temperature are measured by a planar Langmuir probe [LP in Fig. 1(a)] mounted on an axially and radially movable motor system. The probe head can be axially moved to the upstream side at $z = -15$ cm. The estimated electron temperatures for all of the gas species are $\sim 5 \pm 1$ eV at $z = -11$ cm on axis, where we assume a Maxwellian electron energy distribution. The error of the density measurement by the LP is within $\pm 15\%$.

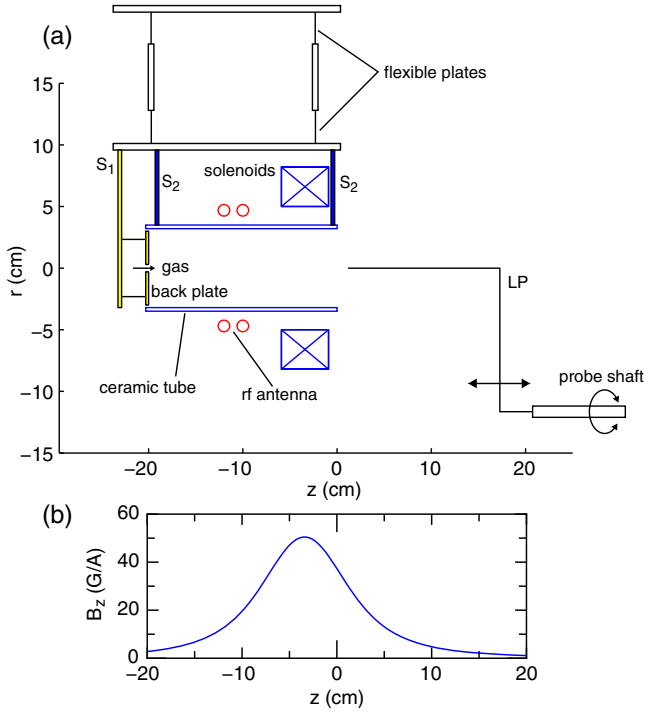

FIG. 1 (color online). (a) Schematic diagram of the experimental setup. (b) Axial profile of the magnetic field strength on axis for $I_B = 1$ A.

Simultaneously with the plasma production, the force exerted by the plasma to the source components, which are attached to the balance, is transferred to the balance; then the displacement is measured by a laser displacement sensor. By attaching only either the source back plate or the ceramic source tube to the balance by using a mechanical support (either S_1 or S_2 shown in Fig. 1), the force components of T_s and T_w can be individually measured. The absolute values of the forces are obtained by multiplying the calibration coefficients. Errors in the force measurements are about $\pm 5\%$ for argon and $\pm 10\%$ for krypton and xenon, where the larger error for the latter cases is due to a thermal issue originating from the higher plasma density, as will be shown later.

The measured T_s and T_w are plotted in Fig. 2(a) by filled and open symbols, respectively, as a function of I_B, where the negative value of the force indicates that the displacement of the balance to the positive z direction is detected and corresponds to the negative effect on the propulsive performance. The sum of the measured T_s and T_w, which corresponds to the axial momentum exhausted from the source, is plotted in Fig. 2(b). Figure 2(c) shows the plasma density measured inside the source cavity as a function of I_B together with fitting curves for visual guides. It is found that the larger values of T_s can be obtained when using the heavier gas species (krypton and xenon), compared with the argon case. According to Ref. [23], T_s corresponds to the integration of the electron pressure in the cross section; the larger values of T_s seem to be due to higher plasma density for the heavier gas species, as shown in Fig. 2(c). The measured T_w for argon shows a negative value for $I_B < 2$ A and a negligible value for $I_B > 2$ A as well as the previous experiment [19], while the significantly negative values of T_w are detected for the krypton and xenon cases for all of the values of I_B. These negative T_w's clearly show that the axial plasma momentum is delivered by the ions lost to the lateral wall, which has never been taken into account in previous thruster models [16,22]. As the value of $T_s + T_w$ in Fig. 2(b) is found to be

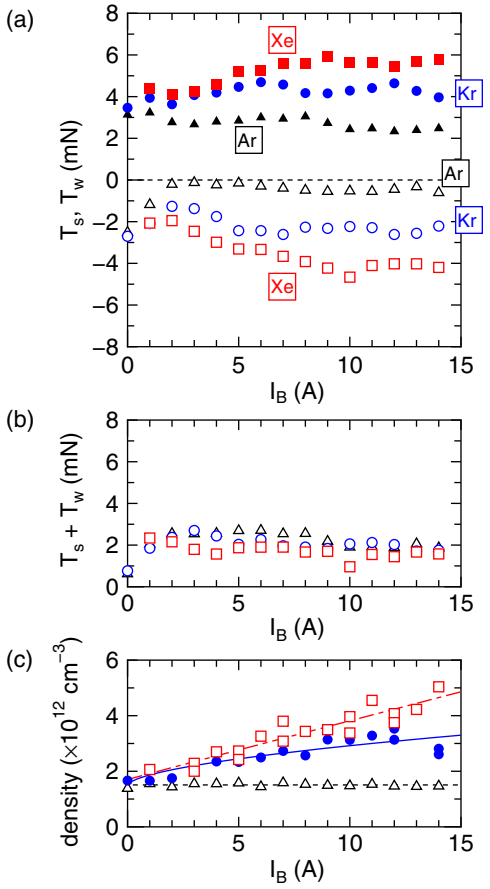

FIG. 2 (color online). (a) Measured forces to the back plate (T_s; filled symbols) and to the lateral wall (T_w; open symbols) as a function of the solenoid current I_B for argon (triangles), krypton (circles), and xenon (squares). (b) Sum of the forces $T_s + T_w$ for argon (open triangles), krypton (open circles), and xenon (open squares). (c) Plasma density versus I_B for the argon ($z = -12$ cm; open triangles), krypton ($z = -11$ cm; filled circles), and xenon ($z = -11$ cm; open squares) cases, where the data for argon are from Ref. [19].

similar for all of the cases and is about 2 to 3 mN, the T_w term significantly affects the thruster performance as well as the T_s term.

Figure 3 shows radial profiles of the plasma density taken at $z = -11$ cm for $I_B = 7$ A. As the density profiles in the source cavity for all of the cases are center peaked, the data can be fairly fitted by the Bessel function of order zero having the first zero position at the lateral wall, as plotted by dotted, solid, and dotted-dashed lines for visual guides in Fig. 3. Therefore the density integrated in the cross section is qualitatively discussed with only the measured density on axis. It should be noted that the axial location of the measurement ($z = -11$ cm) does not give the maximum density for the krypton and xenon cases, as will be shown later in Fig. 4; the absolute values of the T_s term when using the measured density profiles are not discussed here.

Figure 4(a) shows the axial profiles of the plasma density on axis, where the solenoid current is chosen to be

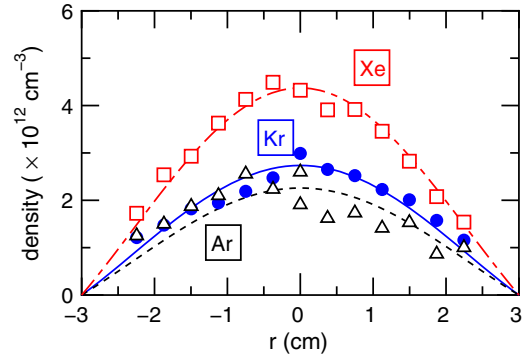

FIG. 3 (color online). Radial profiles of the plasma density taken at $z = -11$ cm for argon (open triangles), krypton (filled circles), and xenon (open squares) for $I_B = 7$ A. The dotted, solid, and dotted-dashed lines are the fitted Bessel functions of order zero for visual guides.

$I_B = 7$ A. The normalized density profiles are also plotted in Fig. 4(b) for discussing the axial decay of the plasma density. The plasma density for argon has a maximum at $z \sim -11$ cm, which is close to both the rf antenna and the axial center of the source. The density gradually decreases and seems to be fairly symmetric along the z axis in the source with respect to the axial center of the source; then T_w is negligible, as shown by the open triangles in Fig. 2. It should be noted that an axially asymmetric density profile having a larger decay of the density near the source exit has been observed for no magnetic field case in the previous experiment [19]; the negative value of T_w is simultaneously detected for $I_B < 2$ A, as seen in Fig. 2(a). For the krypton

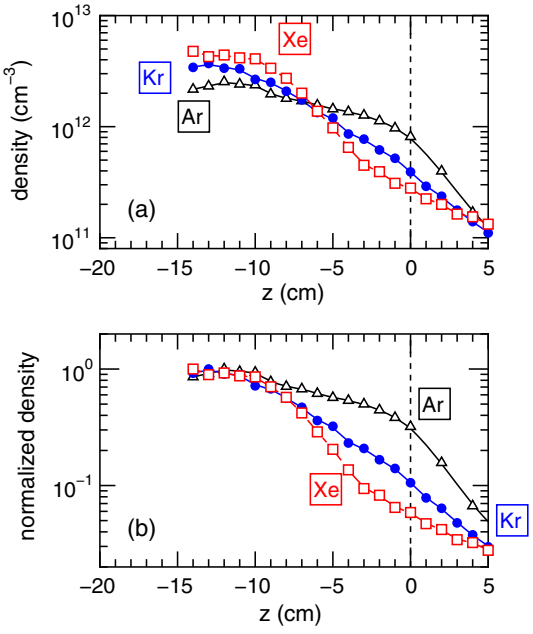

FIG. 4 (color online). Axial profiles of (a) the plasma density and (b) the normalized density for argon (open triangles), krypton (filled circles), and xenon (open squares) for $I_B = 7$ A.

case, the larger density decay is seen at $z \sim -10$–0 cm in Fig. 4(a), which becomes more conspicuous for the xenon case. Furthermore, the maximum density position seems to be shifted to the more upstream side ($z \sim -11$ cm for argon, $z \sim -13$ cm for krypton, and $z < -15$ cm for xenon); i.e., the axial density profile becomes more axially asymmetric with respect to the axial center of the source for the heavier gas species. A similar experimental device has shown that the potential structure following to the Boltzmann relation is formed [24]; hence a larger electric field is expected to be formed for the larger density decay. Such an axial electric field accelerates the ions to the positive z direction and increases their axial momentum. When these ions are lost to the lateral wall, the significant axial momentum is delivered to the lateral wall, which is evidenced by the directly and individually measured negative value of T_w.

Let us assume that the neutral pressure with no plasma in the cavity is double that measured at the chamber side port, according to the conventional vacuum theory [25]: i.e., ~1.4 mTorr for argon, ~1 mTorr for krypton, and ~0.6 mTorr for xenon at the cavity center, respectively. The ionization rate is simply estimated from the plasma density in Fig. 2(c) as ~3% for argon, 5%–10% for krypton, and 7.5%–25% for xenon, respectively. For the weakly ionized argon case, the axially asymmetric density profile for $I_B = 0$ A shown in Ref. [19] is considered to be due to a higher neutral pressure near the back wall. For $I_B \sim 2$ A, giving the magnetic field of ~100 G near the source exit, the ion Larmor radius becomes close to the source radius; then the cross-field diffusion is somewhat inhibited near the solenoid region and the plasma is axially transported. As a result of the increased plasma density near the source exit, the symmetric density profile seen in Fig. 4 can be obtained. Although the ions are still lost to the lateral wall for the magnetic field strength being tested, the significant axial momentum is not transferred to the radially lost ions because of the reductions of the density gradient and the axial electric field. Therefore, the data for argon indicate that the magnetic field inhibits the radial loss of the axial momentum. For the highly ionized krypton and xenon cases, the negative value of T_w is enhanced by an increasing I_B, which is considered to be related to the increased plasma density as well as T_s. However, the inhibition effect by the magnetic field seems to be small. This implies that the neutral depletion effect, rather than the magnetic field effect, is dominant. The previous theories have shown that the axially asymmetric density profile is formed due to the neutral depletion when introducing the gas from the upstream side [15,22]. Actually, the asymmetry for the xenon case with the higher ionization rate is greater than that for the krypton case, as shown in Fig. 4. When increasing the magnetic field strength, the neutral depletion effect seems to be enhanced due to the increased plasma density [Fig. 2(c)]; then the resultant asymmetric profile causes the radial loss of the axial momentum, although some inhibition effect by the magnetic field would simultaneously occur.

In summary, the individual measurement of the axial force exerted on the lateral wall of the HPT is performed for argon, krypton, and xenon gases. The presence of the previously neglected axial momentum transferred to the lateral wall is experimentally detected when the plasma density profile in the source has the axial asymmetry and the strong decay, which is considered to yield the axial electric field and the axial ion acceleration inside the source. The density decay and the loss of the axial momentum are inhibited by applying the magnetic field for the weakly ionized argon case, while the momentum loss is observed to be enhanced by the magnetic field for the highly ionized krypton and xenon cases. The former and latter phenomena are qualitatively interpreted with the competing effects of the magnetic field and the neutral depletion on the axial density profile, respectively. The measurement of the neutral profile is required to verify the neutral depletion effect and still remains a further issue. The presently detected axial momentum lost to the lateral wall provides important information relating to the radial ion flux and the axial ion velocity at the wall boundary. Such a momentum interaction with the physical boundary is a common problem for laboratory bounded plasmas beyond the HPT since the momentum balance affects the plasma characteristics.

This work is partially supported by grants-in-aid for scientific research (Grants No. B 25287150 and No. A 26247096) from the Japan Society for the Promotion of Science and the Yazaki Memorial Foundation for Science and Technology.

*kazunori@ecei.tohoku.ac.jp

[1] D. L. Meier, S. Koide, and Y. Uchida, Science **291**, 84 (2001).
[2] R. E. Ergun, C. W. Carlson, J. P. McFadden, F. S. Mozer, L. Muschietti, I. Roth, and R. J. Strangeway, Phys. Rev. Lett. **81**, 826 (1998).
[3] C. Holland, J. H. Yu, A. James, D. Nishijima, M. Shimada, N. Taheri, and G. R. Tynan, Phys. Rev. Lett. **96**, 195002 (2006).
[4] F. I. Parra, M. Barnes, E. G. Highcock, A. A. Schekochihin, and S. C. Cowley, Phys. Rev. Lett. **106**, 115004 (2011).
[5] A. Fruchtman, G. Makrinich, P. Chabert, and J. M. Rax, Phys. Rev. Lett. **95**, 115002 (2005).
[6] A. Fruchtman, Phys. Rev. Lett. **96**, 065002 (2006).
[7] C. Charles, J. Phys. D **42**, 163001 (2009).
[8] F. F. Chen, Plasma Phys. Controlled Fusion **33**, 339 (1991).
[9] R. W. Boswell and F. F. Chen, IEEE Trans. Plasma Sci. **25**, 1229 (1997).
[10] S. A. Cohen, N. S. Siefert, S. Stange, R. F. Boivin, E. E. Scime, and F. M. Levinton, Phys. Plasmas **10**, 2593 (2003).

[11] C. Charles and R. W. Boswell, Phys. Plasmas **11**, 1706 (2004).
[12] X. Sun, A. M. Keesee, C. Biloiu, E. E. Scime, A. Meige, C. Charles, and R. W. Boswell, Phys. Rev. Lett. **95**, 025004 (2005).
[13] K. Takahashi, T. Lafleur, C. Charles, P. Alexander, and R. W. Boswell, Phys. Rev. Lett. **107**, 235001 (2011).
[14] E. Ahedo and M. Merino, Phys. Plasmas **17**, 073501 (2010).
[15] E. Ahedo and J. Navarro-Cavallé, Phys. Plasmas **20**, 043512 (2013).
[16] T. Lafleur, Phys. Plasmas **21**, 043507 (2014).
[17] A. Fruchtman, Plasma Sources Sci. Technol. **18**, 025033 (2009).
[18] J. M. Little and E. Y. Choueiri, IEEE Trans. Plasma Sci. **43**, 277 (2015).
[19] K. Takahashi, C. Charles, and R. W. Boswell, Phys. Rev. Lett. **110**, 195003 (2013).
[20] S. Yun, K. Taylor, and G. R. Tynan, Phys. Plasmas **7**, 3448 (2000).
[21] R. M. Magee, M. E. Galante, J. Carr, Jr., G. Lusk, D. W. McCarren, and E. E. Scime, Phys. Plasmas **20**, 123511 (2013).
[22] A. Fruchtman, IEEE Trans. Plasma Sci. **36**, 403 (2008).
[23] T. Lafleur, K. Takahashi, C. Charles, and R. W. Boswell, Phys. Plasmas **18**, 080701 (2011).
[24] C. Charles, R. Boswell, and K. Takahashi, Appl. Phys. Lett. **102**, 223510 (2013).
[25] J. F. O'Hanlon, *A User's Guide to Vacuum Technology*, 3rd ed. (John Wiley & Sons, Hobokin, NJ, 2003), p. 34.